Synergistic effect of manganese oxide nanoparticles and graphene nanosheets in composite anodes for lithium ion batteries

Article *in* Materials Research Express · January 2015

DOI: 10.1088/2053-1591/2/1/015503

Synergistic effect of manganese oxide nanoparticles and graphene nanosheets in composite anodes for lithium ion batteries

2015 Mater. Res. Express 2 015503

(http://iopscience.iop.org/2053-1591/2/1/015503)

Materials Research Express

PAPER

Synergistic effect of manganese oxide nanoparticles and graphene nanosheets in composite anodes for lithium ion batteries

RECEIVED
10 September 2014

ACCEPTED FOR PUBLICATION
8 December 2014

PUBLISHED
9 January 2015

Shu Luo[1,2], **Yang Yu**[1,2], **Mengya Li**[1], **Hengcai Wu**[1], **Fei Zhao**[1], **Kaili Jiang**[1], **Jiaping Wang**[1], **Feiyu Kang**[2] **and Shoushan Fan**[1,2]

[1] Department of Physics and Tsinghua-Foxconn Nanotechnology Research Center, Tsinghua University, Beijing, People's Republic of China

[2] School of Materials Science and Engineering, Tsinghua University, Beijing, People's Republic of China

E-mail: jpwang@tsinghua.edu.cn

Keywords: synergistic effect, manganese oxide, graphene nanosheet, anode, lithium ion battery

Abstract

A graphene-Mn_3O_4-graphene (GMG) sandwich structure with homogeneous anchoring of Mn_3O_4 nanoparticles among flexible and conductive graphene nanosheets (GSs) is achieved through dispersion of the GSs in $Mn(NO_3)_2$ solution and subsequent calcination. Mn_3O_4 nanoparticles are $50 \sim 200$ nm clusters consisting of $10 \sim 20$ nm primary particles, and serve as spacers to prevent the restacking of the GSs. GSs provide a highly conductive network among Mn_3O_4 nanoparticles for efficient electron transfer and buffer any volume change during cycling. Due to the strong synergistic effect between Mn_3O_4 and GSs, the capacity contributions from GSs and Mn_3O_4 in GMG are much larger than capacities of pure GSs and Mn_3O_4. Consequently, the GMG composite electrodes show excellent electrochemical properties for lithium ion battery applications, demonstrating a large reversible capacity of 750 mAh g^{-1} at 0.1 C based on the mass of GMG with no capacity fading after 100 cycles, and high rate abilities of 500 mAh g^{-1} at 5 C and 380 mAh g^{-1} at 10 C.

1. Introduction

Lithium ion batteries (LIBs) have long been regarded as the most promising power source for electrical vehicles (EVs). However, to meet the demands of EVs, the energy and power densities of LIBs still need to be improved. Since 2000, transition metal oxides have been studied extensively as anode materials for LIBs because of their high theoretical capacities based on the reaction of $MO + 2e^- + 2Li^+ \leftrightarrow M + Li_2O$ [1–5]. Among all the transition metal oxides, Mn_3O_4 has attracted more and more attention recently owing to its high theoretical capacity (936 mAh g^{-1}, 2.5 times the capacity of graphite), low cost, and environmental friendly essence [6–8]. However, the electrochemical properties of Mn_3O_4 are often restricted by its low conductivity ($10^{-8} \sim 10^{-7}$ S cm^{-1}) [9], large volume change, and severe particle aggregation through cycling, which would lead to cracking and pulverization of the electrode. As a result, pure Mn_3O_4 often suffers from large irreversible capacity loss and rapid capacity fading [10, 11]. Many efforts have been made to solve these problems, and one of the most effective strategies is to combine Mn_3O_4 nanostructures with carbon materials [11–18]. Nanostructured electrode materials have the advantage of large contact area with electrolyte, short diffusion length of Li^+, and small reactive barrier over their bulk counterparts [19, 20]. Meanwhile, the use of carbon material as conductive matrix has been proved as an effective way to improve the electron transfer ability in the composite electrode. Therefore, great improvements in electrochemical performance by designing various Mn_3O_4/carbon nanocomposites have been reported in literature.

Graphene is an excellent substrate to hold active nanomaterials for energy storage [21–23] because of its superior conductivity, flexibility, large surface area, and chemical stability [24–26]. Multilayer graphene nanosheets (GSs), which are composed of limited layers of graphene, can be obtained in a much cheaper and more large-scale way than single layer graphene [27], while still keeping the advantages of graphene mentioned above. Many attempts have been made to use GSs as the conductive framework to form composite electrodes,

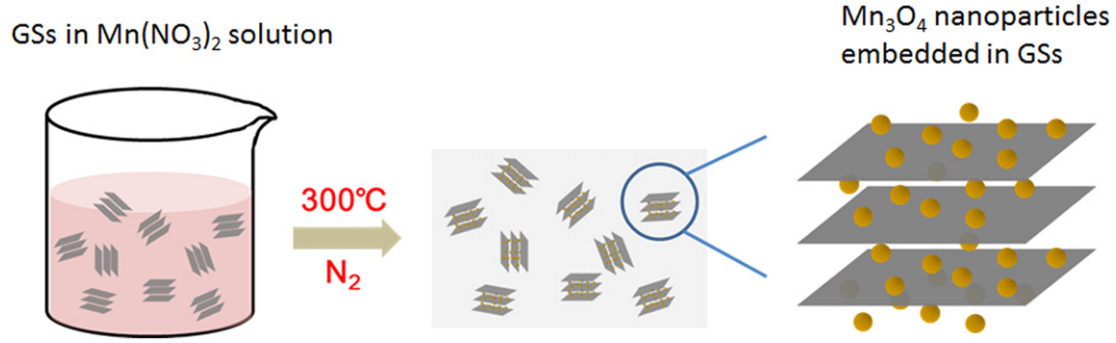

Figure 1. Schematic illustration of the synthesis of GMG composite.

such as MnO/GSs [28], MoS_2/GSs [29], S/GSs [30] and so on, in order to achieve improved electrochemical performance. In addition to its capability as conductive and flexible support for anchoring well-dispersed nanoparticles, GSs can also effectively limit the volume expansion/contraction and prevent the aggregation of nanoparticles during the Li^+ insertion/extraction processes. Meanwhile, nanoparticles embedded among GSs can suppress the re-stacking of graphene layers and consequently maintain their high active surface area. As a result, in the nanoparticle-GS composite electrodes, both nanoparticles and GSs can present improved electrochemical performance over the electrodes with only nanoparticles or GSs as active material. The hypothesis of synergistic effect between nanoparticles and GSs has been suggested to explain the improved performance of MnO-GS, MoS_2-GS, and Co_3O_4-GS composites [28, 29, 31]. However, further discussions on quantitative analysis of such synergistic effect are still much needed.

Herein, we quantitatively study the synergistic effect in graphene-Mn_3O_4 nanoparticle-graphene (GMG) sandwich structure obtained by dispersion of GSs in $Mn(NO_3)_2$ solution and subsequent calcination. The structure and composition of GMG composite electrodes are characterized by scanning electron microscopy (SEM), transmission electron microscopy (TEM), x-ray diffraction (XRD), Raman spectroscopy, and thermal gravimetric analysis (TGA). The electrochemical performances of the GMG composite electrodes are measured by galvanostatic charge and discharge tests at various current densities. The GMG composite electrodes show excellent electrochemical properties for lithium ion battery applications, demonstrating a large reversible capacity of 750 mAh g^{-1} at 0.1 C based on the mass of GMG with no capacity fading after 100 cycles, and high rate abilities of 500 mAh g^{-1} at 5 C and 380 mAh g^{-1} at 10 C. The synergistic effect between GSs and Mn_3O_4 in GMG composite electrode is clearly demonstrated by comparing the capacity contributions from GSs and Mn_3O_4 in GMG and the capacities of pure GSs and Mn_3O_4. The excellent electrochemical performances of the GMG composite electrodes are ascribed to such a synergistic effect.

2. Methods

2.1. Fabrication of GSs and GMG composites

Natural graphite flakes were first transformed into expandable graphite by acid treatment in the mixture of H_2SO_4 (98 wt%) and H_2O_2 (30 wt%) and thermal exfoliation. More details on the synthesis of expandable graphite can be found in literature [32]. The expandable graphite was then subjected to slicing by high-pressure airflow and subsequent exfoliation by ultrasonication in N-methyl-2-pyrrolidone (NMP) suspension (0.1 mg mL^{-1}). The product would be GSs with limited layers of graphene. Figure 1 illustrates the preparation of the GMG composite. A controlled amount of GSs were added into 50 wt% $Mn(NO_3)_2$ water solution, with the molar ratio of C:Mn = 10:1. Then the mixture was stirred at a rate of 400 r min^{-1} at 80 °C until the water in the mixture was completely evaporated. Finally, the dried mixture was ground into fine powder and then calcinated in a silicon tube at 300 °C in N_2 for 1 h to obtain the GMG composite, with oxide nanoparticles homogeneously anchored on GSs.

2.2. Morphology and structure characterization

Microstructures of the GMG composites were characterized using an FEI Sirion200 scanning electron microscope (SEM) operating at 10 kV and an FEI Tecnai G2F20 transmission electron microscope (TEM) operating at 200 kV. Powder x-ray diffraction (XRD) data of the GMG sample was collected on a Rigaku D/max 2500PC diffractometer operating at 40 kV and 200 mA with Cu Kα_1 radiation in θ–2 θ diffraction geometry, with a 2 θ range of 10–90°. X-ray photoelectron spectroscopy (XPS) was performed to analyze the oxidation

states and the spectra were collected on a Thermal Escalab 250xi spectrometer operating at 50 kV. Thermal gravimetric analysis (TGA) test was conducted using a Pyris 1 TGA (Perkin Elmer, USA) at a heating rate of 10 °C min^{-1} between 25 and 800 °C in air. GS powders were pressed into a pellet with an applied pressure of 4 MPa, and its conductivity was measured on a Resmap four-probe system (Creative Design Engineering Inc., USA).

2.3. Electrochemical test

The working electrode was prepared from a mixing paste of 80 wt% of GMG, 10 wt% Super P, and 10 wt% poly (vinylidene fluoride) binder in NMP. The paste was coated onto a copper foil, and then dried under vacuum at 120 °C for 24 h. Coin-type (CR2016) half-cells were assembled in an Ar-filled glove box (M. Braun inert gas systems Co. Ltd) with GMG composite as the working electrode, a porous polymer film (Celgard 2400, USA) as the separator, and Li metal as the negative electrode. 1 M $LiPF_6$ solution in ethylene carbonate (EC) and diethyl carbonate (DEC) mixed at weight ratio of 1:1 was used as electrolyte. The cells were tested using a Land battery test system (Wuhan Land Electronic Co., China) with cut-off voltages of 0.01–3 V at room temperature. The cyclic voltammetry (CV) study was conducted using an electrochemical workstation (PARSTAT 2273) between 0.01 and 3 V at a scan rate of 0.1 mV s^{-1}.

3. Results and discussion

GMG composites were obtained through dispersion of the GSs in the $Mn(NO_3)_2$ water solution and subsequent transformation of $Mn(NO_3)_2$/GSs into GMG composite by calcination at 300 °C in N_2, with oxide nanoparticles homogeneously anchored on GSs. As shown in the XRD pattern (figure 2(a)), the obtained GMG composite has a very sharp and high peak around 26° as well as a small peak at 54.7°, which can be indexed into (002) and (004) planes of graphene. These results indicate that GSs retain their crystalline structure after anchoring oxide nanoparticles. Raman spectrum in figure 2(b) shows that the peak at 648 cm^{-1} is attributed to Mn_3O_4 [33] and the peaks at 1353 cm^{-1} and 1577 cm^{-1} are the D band and G band of GSs. The G band is much higher than the D band, corresponding to $I_G/I_D \sim 5.7$, suggesting that GSs contain a limited amount of defects, consistent with the XRD result. Therefore, the high conductivity of GSs (8×10^2 S cm^{-1}) is expected to be preserved in GMG, and GSs can work as a conductive substrate for Mn_3O_4 nanoparticles. In the XRD pattern, peaks of the Mn_3O_4 are quite weak compared with those of GSs, probably due to the low content of Mn_3O_4 in GMG. Figure 2(c) is a magnified XRD pattern with a 2θ range of 30° to 90°, which can be clearly indexed as the Mn_3O_4 phase (JCPDS 24-0734), with the main diffraction peaks (103), (211) and (224) of Mn_3O_4 relatively sharp. The small peak around 41° can be attributed to the limited amount of MnO phase (75-0625). The XPS spectra in figure 2(d) shows that the binding energy of Mn $2p_{3/2}$ and Mn $2p_{1/2}$ is 641.7 eV and 653.4 eV, respectively, which means the spin–orbit splitting between the Mn $2p_{3/2}$ and Mn $2p_{1/2}$ level is 11.7 eV. This matches with the results of Mn_3O_4 reported previously in the literature [34, 35]. The TGA result of the GMG composite tested in air from 25 °C to 1000 °C is shown in figure 2(e). As GSs gradually burned away from 500 °C to 900 °C, the final product would be pure Mn_3O_4 when heated to 1000 °C [36]. The content of Mn_3O_4 in GMG is 25 wt%.

Figure 3 shows the SEM and TEM images of GSs and GMG composite. The graphene layers in GSs loosely stacked together, providing sufficient space and large surface area for inserting and anchoring nanoparticles. As shown in the microstructure of GMG composite (figures 3(c) and (d)), the multi-layer structure and large surface of GSs are well-preserved after the insertion of Mn_3O_4 nanoparticles. Mn_3O_4 nanoparticles are homogeneously dispersed among the graphene layers, achieving a graphene–Mn_3O_4–graphene sandwich structure. The particle size of Mn_3O_4 can be identified as 50 ~ 200 nm from the SEM image of GMG. The TEM image (figure 3(d)) further illustrates that primary Mn_3O_4 particles (10 ~ 20 nm) with clear crystalline planes assemble into porous clusters of 50 ~ 200 nm. With the small particle size and the close contact between Mn_3O_4 nanoparticles and GSs, electrons produced in Mn_3O_4 nanoparticles through cycling can be easily transferred through the neighboring GSs, and Li^+ ions can readily diffuse through the channels among GSs and the pores in the Mn_3O_4 clusters, resulting in improved lithium storage capacity and rate performance of the GMG composite.

Figure 4 illustrates the cycle and rate performance of GMG composites, GSs, and commercial Mn_3O_4 nanoparticles with size of 50 nm. The electrochemical properties of GMG are much better than GSs and commercial Mn_3O_4 nanoparticles. The GMG electrode exhibits capacities of 905 mAh g^{-1} and 750 mAh g^{-1} (based on the mass of GMG composite) at 0.1 C for the 1st and 2nd cycle with the Coulombic efficiency of 74%, and shows no obvious fading during the following cycles. Even after 100 cycles at 0.1 C, the GMG electrode still presents 100% capacity retention, and the Coulombic efficiency keeps stable at 97.5%. On the contrary, the GS electrode only exhibits a stable capacity of as low as 370 mAh g^{-1}. The electrode made with commercial Mn_3O_4 nanoparticles displays a high initial capacity of 1035 mAh g^{-1} for the 1st cycle, however, rapid capacity fading

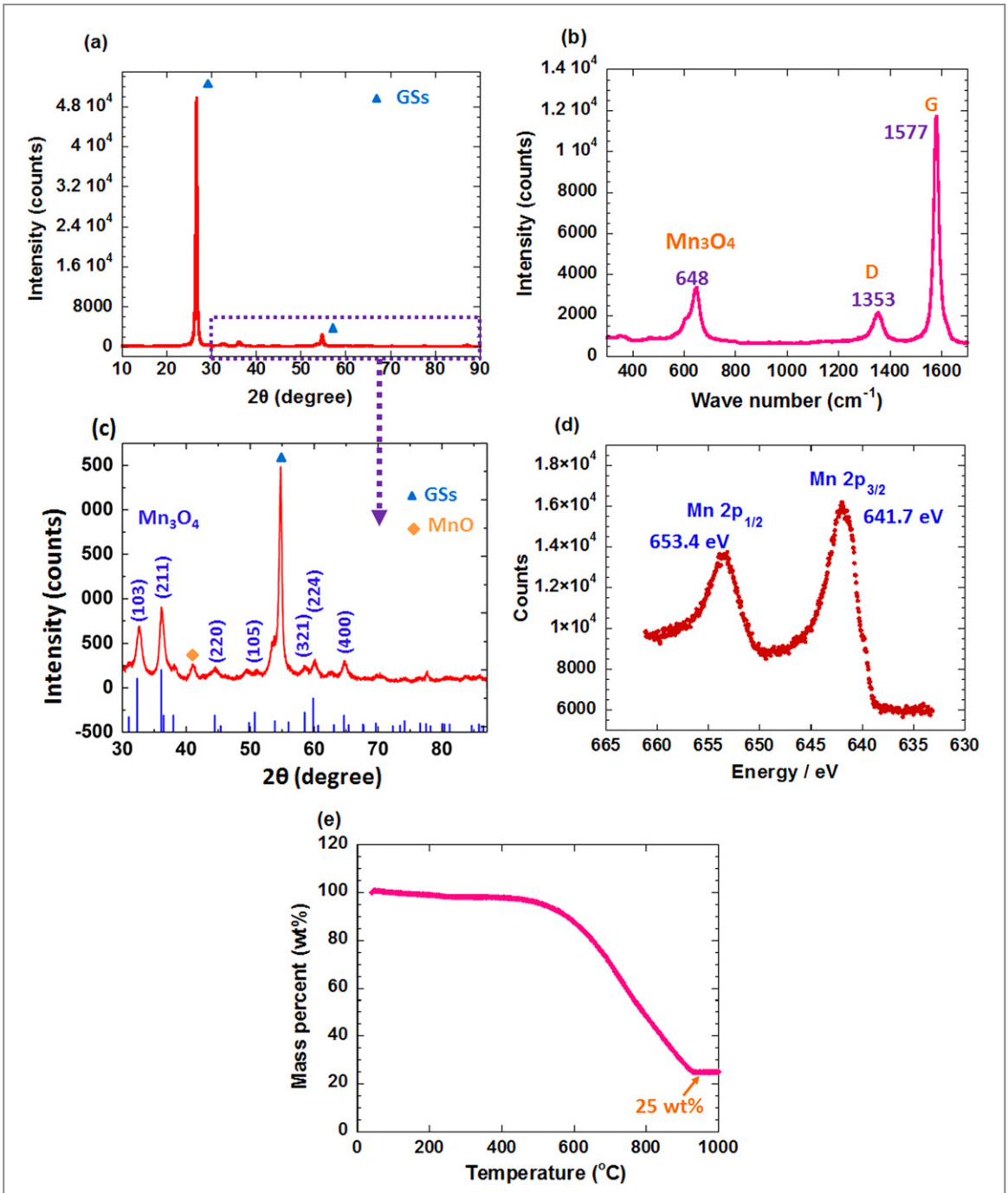

Figure 2. (a) XRD pattern, (b) Raman spectrum, (c) magnified XRD pattern with a 2 θ range of 30 ~ 90°, (d) XPS spectra of Mn 2p, and (d) TGA result of the GMG composite.

occurs for the following cycles. The rate performance of the GMG composite is also outstanding, with capacities of 500 mAh g^{-1} at 5 C and 380 mAh g^{-1} at 10 C. While for GSs, the capacities are only 290 mAh g^{-1} at 5 C and 190 mAh g^{-1} at 10 C. Rate performance of Mn_3O_4 nanoparticles is even worse, with capacities of only 175 mAh g^{-1} at 5 C and 80 mAh g^{-1} at 10 C. These results demonstrate that the electrochemical performances of pure GSs and Mn_3O_4 nanoparticles are not satisfactory. However, the combination of GSs and Mn_3O_4 nanoparticles into the GMG composite can result in enhanced electrochemical performance.

To investigate the mechanism of the enhanced performance of GMG, the discharge curves (at 0.1 C) of GSs, commercial Mn_3O_4 nanoparticles, and GMG are compared in figure 5. GSs have a typical discharge curve of graphite with a small slope between 0.1–0.2 V as well as a long plateau at 0.1 V, and this voltage window below 0.2 V is named as range A. (figure 5(a)). Mn_3O_4 has a plateau around 0.5 V for the reduction of oxidized Mn into metallic Mn nanoclusters (figure 5(b)) [37], and this plateau around 0.5 V is named as range B (0.45–0.55 V). Mn_3O_4 also contains a slope below the plateau at 0.5 V, probably caused by an interfacial charging mechanism [38], and often contributes a capacity of only 100 ~ 200 mAh g^{-1} [3, 39]. As for the discharge curve of GMG

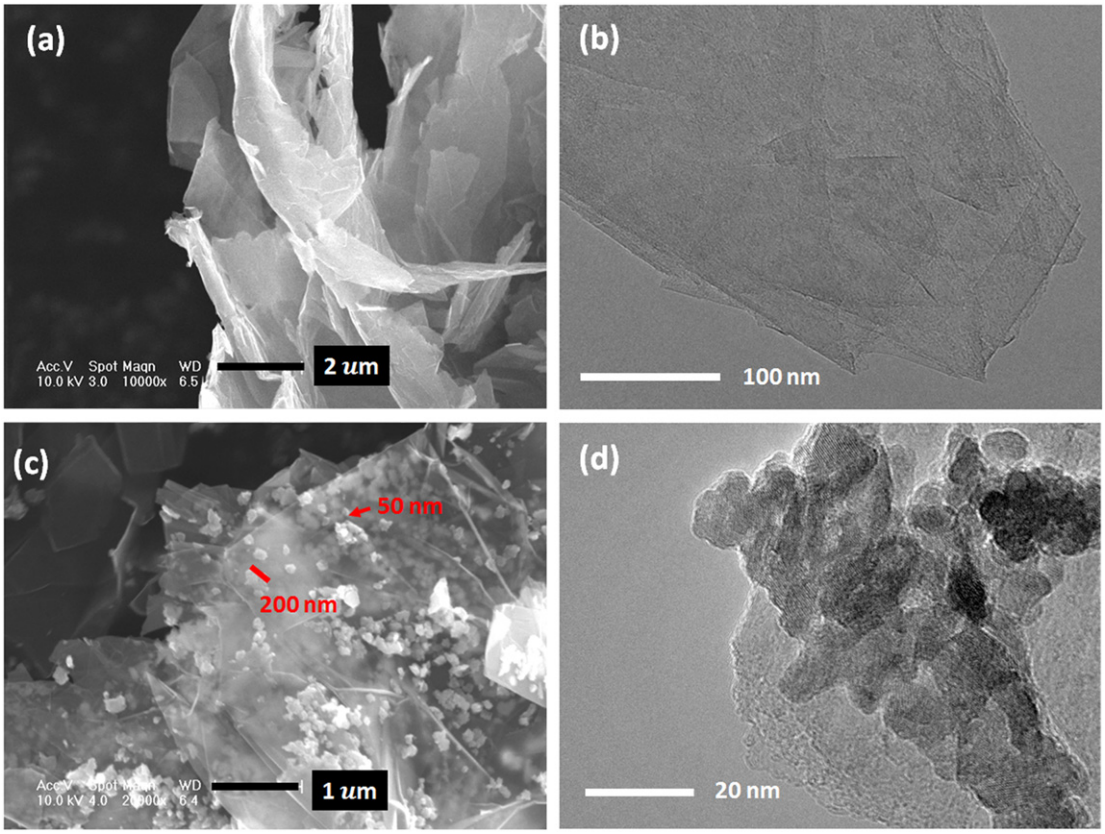

Figure 3. (a), (c) SEM images of GSs and GMG composite, (b), (d) TEM images of GSs and GMG composite.

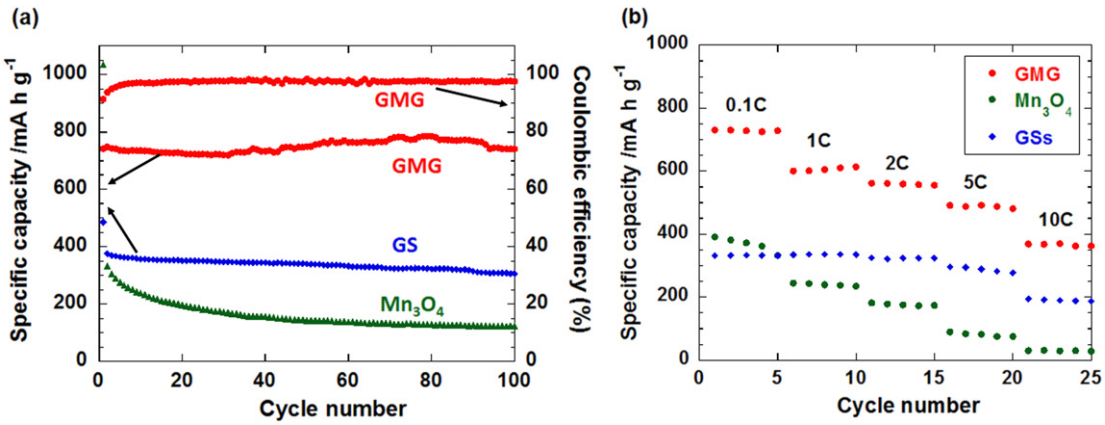

Figure 4. (a) Cycle performance at 0.1 C and (b) rate capability of the GMG composite, GSs, and commercial Mn_3O_4 nanoparticles.

(figure 5(c)), it shows a plateau at 0.5 V for Mn_3O_4 (range B), and a small slope between 0.1–0.2 V and a long plateau at 0.1 V for GSs (range A). Therefore, the discharge curve of the GMG composite can be regarded as the combination of the discharge curves of GSs and Mn_3O_4. This can be further confirmed by the CV curve (2nd cycle) of GMG composite in figure 5(d). It shows a sharp reduction peak around 0.1 V with a small shoulder at 0.2 V for GSs, corresponding to range A in the discharge curve, and a clear reduction peak of Mn_3O_4 at 0.4 V (different from the plateau at 0.5 V of the discharge curve, which is common for Mn_3O_4 composite anode [35]), corresponding to range B in the discharge curve. In the anodic process, the sharp peak at 0.2 V represents the oxidation of GSs, while the broad peaks at 1.3 V and 2.2 V represent the oxidation of Mn° to Mn^{2+} and further oxidation of Mn^{2+} to Mn^{3+} respectively [15]. To study the separate contribution of GSs and Mn_3O_4 to the total capacity of GMG, the capacity in range A in GMG can be attributed to the contribution from GSs, and the capacity in range B in GMG can be attributed to the contribution from Mn_3O_4, as illustrated in figure 5. This

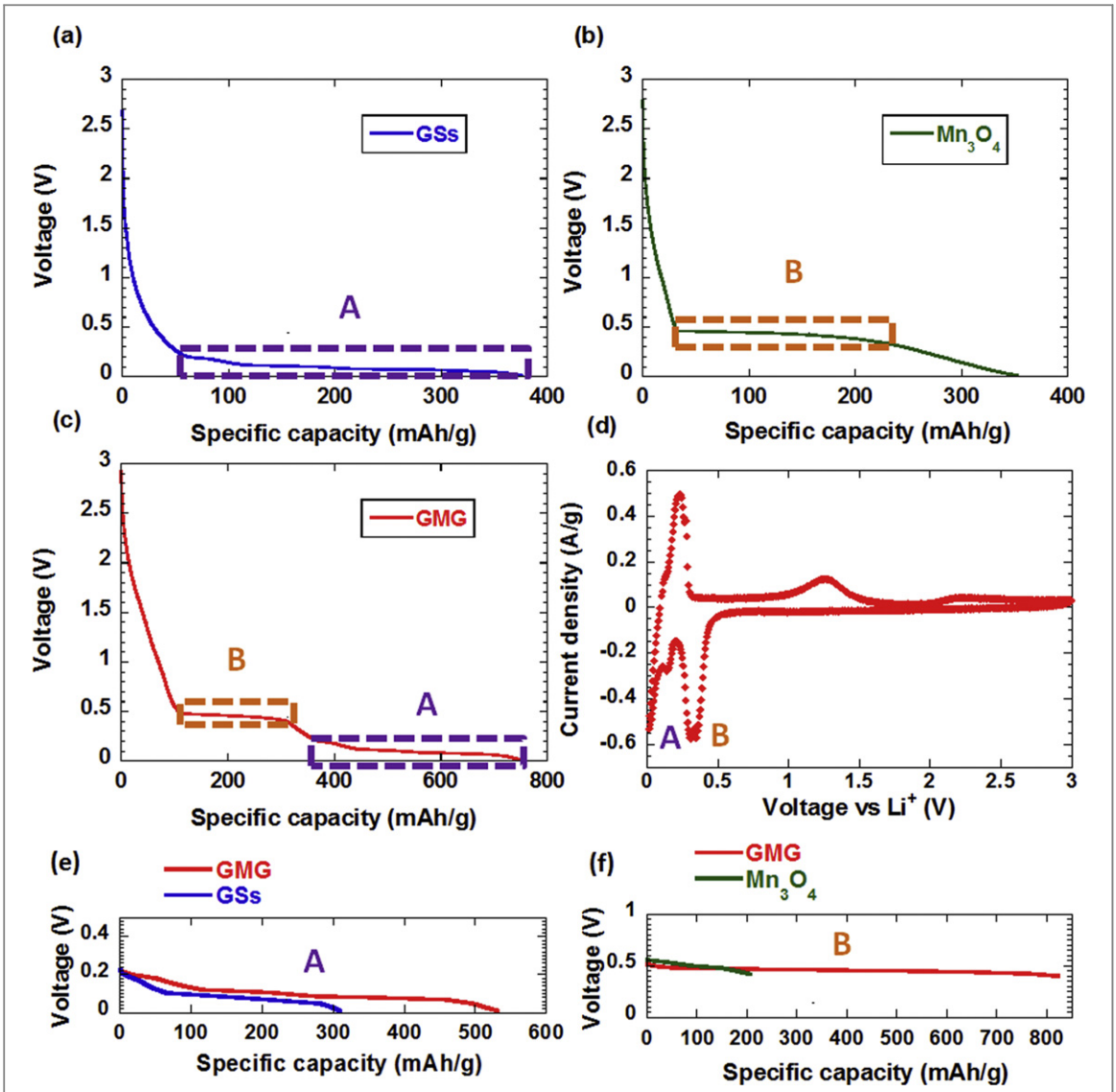

Figure 5. Discharge curves at the second cycle of (a) GSs, (b) commercial Mn_3O_4 nanoparticles, and (c) GMG composite at 0.1 C. The capacity contributions from GSs and Mn_3O_4 are labeled as ranges A (below 0.2 V) and B (0.4–0.55 V). (d) CV curve of the GMG composite at the 2nd cycle. Comparison of the capacities of d) GSs and GMG in range A, and e) commercial Mn_3O_4 and GMG in range B.

could be a rough but convenient way to separately evaluate the capacities of GSs and Mn_3O_4 in GMG. The capacities of GSs in GMG and pure GSs at voltage below 0.2 V (range A) are compared in figure 5(e). GSs in GMG display a capacity of 530 mAh g^{-1} after normalization of the mass of active material. In contrast, pure GSs can only deliver 310 mAh g^{-1} at the same current density. Figure 5(f) shows that at voltage range of 0.45–0.55 V (range B), Mn_3O_4 in GMG shows a capacity of 830 mAh g^{-1} after mass normalization, which is much higher than that of pure Mn_3O_4 (210 mAh g^{-1}).

The enhancement of reversible capacities of both Mn_3O_4 nanoparticles and GSs in the GMG composite can be attributed to the synergistic effect between Mn_3O_4 nanoparticles and GSs. For GSs in GMG, Mn_3O_4 nanoparticles anchored on the graphene layers serve as spacers, protecting them from agglomeration into tightly stacked graphite. The preservation of the separated layer structure in GSs leads to large contact area between graphene layers and electrolyte, and consequently increases the capacity of GSs in the GMG composite. As for the Mn_3O_4 nanoparticles in GMG, GSs not only provide a conductive and flexible substrate for homogeneous anchoring of Mn_3O_4 nanoparticles, but also limit the volume expansion/contraction and prevent the agglomeration of Mn_3O_4 nanoparticles upon cycling. It is the strong synergistic effect between Mn_3O_4 nanoparticles and GSs in GMG that leads to the outstanding electrochemical performance of the GMG composites.

The rate performance of the GMG composite is also compared with some of the best results reported in literature. As shown in table 1, although the capacities of GMG at 1 C to 5 C are not the highest values ever reported, the capacity at 10 C is much higher than that in literature, showing its advantage as a high-rate anode

Table 1. Comparison of the rate performance in this paper with some of the best results in literature.

	Composite/ microstructure	Conductive agent in electrode (wt%)	1 C (mAh g^{-1})	2 C (mAh g^{-1})	5 C (mAh g^{-1})	10 C (mAh g^{-1})
This paper	GMG	10	610	560	500	380
Ref. [15]	Mn_3O_4 hollow sphere	15	830	700	520	300
Ref. [17]	Mn_3O_4/ VGCF	15	730	610	390	
Ref. [40]	Mn_3O_4/N-doped graphene	15	520	382		
Ref. [13]	Mn_3O_4/ graphene	10	400	230		

material to stand super-fast charge/discharge cycles. Considering the less content of conductive additive in the GMG composite electrode, it is suggested that the rate performance of GMG can be further improved with increasing conductive additive.

The good electrochemical performances of the GMG composites benefit from the following aspects: (1) GSs in GMG possess high electrical conductivity, which provide conductive channels among Mn_3O_4 nanoparticles. (2) Both Mn_3O_4 nanoparticles and GSs contain a large surface area for efficient contact with electrolyte and can provide short diffusion distance for Li^+ ion transportation, which are essential for fast and stable Li^+ insertion/ extraction. (3) Most importantly, due to the strong synergistic effect between GSs and Mn_3O_4 nanoparticles, the capacity contributions from GSs and Mn_3O_4 in GMG are much larger than capacities of pure GSs and Mn_3O_4.

4. Conclusion

GMG sandwich structure is developed by uniformly anchoring Mn_3O_4 nanoclusters on flexible and conductive graphene sheets through dispersion of the GSs in $Mn(NO_3)_2$ solution and subsequent calcination. In the GMG composite, graphene layers can provide a conductive channel and also serve as flexible buffer for Mn_3O_4 nanoparticles, therefore, the reversible capacity of Mn_3O_4 nanoparticles can be greatly improved compared with pure Mn_3O_4. On the other hand, Mn_3O_4 nanoparticles in GMG can act as spacers to prevent the re-stacking of the neighboring graphene layers and to increase the surface area of GSs, thus the reversible capacity of GSs in GMG is also improved compared with pure GSs. Due to the strong synergistic effect between Mn_3O_4 nanoparticles and GSs, the electrochemical performance of GMG is very appealing, with a large reversible capacity of 750 mAh g^{-1} at 0.1 C based on the total mass and 100% capacity retention after 100 cycles, and excellent rate capacities of 500 mAh g^{-1} at 5 C and 380 mAh g^{-1} at 10 C.

Acknowledgments

This work was supported by the National Basic Research Program of China (2012CB932301) and National Natural Science Foundation of China (51102146 and 51472141).

References

[1] Poizot P, Laruelle S, Grugeon S, Dupont L and Tarascon J M 2000 *Nature* **407** 496–9
[2] Li H, Richter G and Maier J 2003 *Adv. Mater.* **15** 736–9
[3] Balaya P, Li H, Kienle L and Maier J 2003 *Adv. Funct. Mater.* **13** 621–5
[4] Bruce P G, Scrosati B and Tarascon J M 2008 *Angew. Chem. Int. Ed.* **47** 2930–46
[5] Cabana J, Monconduit L, Larcher D and Palacin M R 2010 *Adv. Mater.* **22** E170–92
[6] Wang J Z, Du N, Wu H, Zhang H, Yu J X and Yang D R 2013 *J. Power Sources* **222** 32–7
[7] Gao J, Lowe M A and Abruna H D 2011 *Chem. Mater.* **23** 3223–7
[8] Yue J, Gu X, Chen L, Wang N, Jiang X, Xu H, Yang J and Qian Y 2014 *J. Mater. Chem.* A **2** 17421–6
[9] Chae C, Kim J H, Kim J M, Sun Y K and Lee J K 2012 *J. Mater. Chem.* **22** 17870–7
[10] Pasero D, Reeves N and West A R 2005 *J. Power Sources* **141** 156–8
[11] Wang H L, Cui L F, Yang Y A, Casalongue H S, Robinson J T, Liang Y Y, Cui Y and Dai H J 2010 *J. Am. Chem. Soc.* **132** 13978–80
[12] Lavoie N, Malenfant P, Courtel F M, Abu-Lebdeh Y and Davidson I J 2012 *J. Power Sources* **213** 249–54
[13] Li L, Guo Z P, Du A J and Liu H K 2012 *J. Mater. Chem.* **22** 3600–5
[14] Luo S, Wu H, Wu Y, Jiang K, Wang J and Fan S 2014 *J. Power Sources* **249** 463–9
[15] Jian G Q, Xu Y H, Lai L C, Wang C S and Zachariah M R 2014 *J. Mater. Chem.* A **2** 4627–32
[16] Deng Y F, Wan L N, Xie Y, Qin X S and Chen G H 2014 *RSC Adv.* **4** 23914–35
[17] Ma F, Yuan A and Xu J 2014 *ACS Appl. Mater. Interfaces* **6** 18129–38

[18] Luo Y, Fan S, Hao N, Zhong S and Liu W 2014 *Dalton Trans.* **43** 15317–20
[19] Larcher D, Masquelier C, Bonnin D, Chabre Y, Masson V, Leriche J B and Tarascon J M 2003 *J. Electrochem. Soc.* **150** A133–9
[20] Zhong K, Xia X, Zhang B, Li H, Wang Z and Chen L 2010 *J. Power Sources* **195** 3300–8
[21] Jang B Z, Liu C G, Neff D, Yu Z N, Wang M C, Xiong W and Zhamu A 2011 *Nano Lett.* **11** 3785–91
[22] Brownson D A C, Kampouris D K and Banks C E 2011 *J. Power Sources* **196** 4873–85
[23] Latorre-Sanchez M, Atienzar P, Abellan G, Puche M, Fornes V, Ribera A and Garcia H 2012 *Carbon* **50** 518–25
[24] Novoselov K S, Geim A K, Morozov S V, Jiang D, Katsnelson M I, Grigorieva I V, Dubonos S V and Firsov A A 2005 *Nature* **438** 197–200
[25] Novoselov K S, Geim A K, Morozov S V, Jiang D, Zhang Y, Dubonos S V, Grigorieva I V and Firsov A A 2004 *Science* **306** 666–9
[26] Geim A K 2009 *Science* **324** 1530–4
[27] Stankovich S, Dikin D A, Piner R D, Kohlhaas K A, Kleinhammes A, Jia Y, Wu Y, Nguyen S T and Ruoff R S 2007 *Carbon* **45** 1558–65
[28] Zhang K J *et al* 2012 *ACS Appl. Mater. Interfaces* 4, 658–64
[29] Zhou X, Wan L and Guo Y 2013 *Chem. Commun.* **49** 1838–40
[30] Ding B, Yuan C, Shen L, Xu G, Nie P, Lai Q and Zhang X 2013 *J. Mater. Chem.* A **1** 1096–101
[31] Wu Z S, Ren W C, Wen L, Gao L B, Zhao J P, Chen Z P, Zhou G M, Li F and Cheng H M 2010 *ACS Nano* **4** 3187–94
[32] Zou L, Kang F, Zheng Y and Shen W 2009 *Electrochim. Acta* **54** 3930–4
[33] Bussamara R, Melo W W M, Scholten J D, Migowski P, Marin G, Zapata M J M, Machado G, Teixeira S R, Novak M A and Dupont J 2013 *Dalton Trans.* **42** 14473–9
[34] Dubal D P and Holze R 2012 *RSC Adv.* **2** 12096–100
[35] Xu S, Zhu Y, Zhuang Q and Wu C 2013 *Mater. Res. Bull.* **48** 3479–84
[36] Berbenni V and Marini A 2003 *Mater. Res. Bull.* **38** 1859–66
[37] Fang X P, Lu X, Guo X W, Mao Y, Hu Y S, Wang J Z, Wang Z X, Wu F, Liu H K and Chen L Q 2010 *Electrochem. Commun.* **12** 1520–3
[38] Jamnik J and Maier J 2003 *Phys. Chem. Chem. Phys.* **5** 5215–20
[39] Laruelle S, Grugeon S, Poizot P, Dolle M, Dupont L and Tarascon J M 2002 *J. Electrochem. Soc.* **149** A627–34
[40] Park S K, Jin A, Yu S H, Ha J, Jang B, Bong S, Woo S, Sung Y E and Piao Y 2014 *Electrochim. Acta* **120** 452–9